Electronic Supplementary Information (ESI)

High-Capacity Sieving of C_3F_6 and C_3F_8 by a Copper-Based MOF with Interconnected Gourd-Shaped Channels†

Zijian Wang[ab], Mu-Yang Zhou[b], Shanshan Mao[b], Yilu Wu[b], Shenfang Li[ab], Xin Zhou[b], Fu-An Guo[ab], Liang Yu*[b], Manglai Gao*[ac], and Hao Wang*[b]

[a]State Key Laboratory of Heavy Oil Processing, College of Science, China University of Petroleum, Beijing 102249, P.R. China.

[b]Hoffmann Institute of Advanced Materials, Shenzhen Polytechnic 7098 Liuxian Blvd., Nanshan District, Shenzhen, Guangdong 518055, P. R. China.

[c]Liaoning Petrochemical University，No.1 West Section of Dandong Road, Wanghua District, Fushun City, Liaoning Province, 113001, China.

Supplementary Methods

General characterizations

All commercially available reagents were used as received without further purification. Powder X-ray diffraction (PXRD) and in-situ PXRD patterns were collected on a Bruker D8 Advance diffractometer using Cu Kα radiation (λ = 1.54056Å) at 40 kV and 40 mA. Thermogravimetric analysis (TGA) was performed on a TA Instruments TGA550 analyzer. Samples (ca. 4-5 mg) were heated from room temperature to 600 °C at a heating rate of 10 °C min^{-1}. Thermogravimetric measurements were performed on a thermal analyzer (TGA 550, TA Instruments) in N_2 atmosphere, and the ramping rate was 10 °C/min. Scanning electron micrographs (SEM) images were taken using a JEOL JSM-IT800 (SHL). C_3F_6, and C_3F_8 adsorption isotherms were measured on a Micromeritics 3Flex analyzer. The N_2 adsorption-desorption isotherms at 77 K were measured on a Micromeritics 3Flex analyzer. The Brunauer-Emmett-Teller (BET) surface area was evaluated by strictly applying the four Rouquerol criteria to select the appropriate relative pressure range. Furthermore, the pore size distribution (PSD) was derived using the Non-Local Density Functional Theory (NLDFT) method embedded in the instrument's built-in software (2D-NLDFT, N_2-Carbon Finite Pores, As=6). For each adsorption experiment, ~100 mg of MOF sample was activated 12 hours prior to data collection.

Synthesis of CuHTPO

The synthesis of **CuHTPO** was carried out based on a previously reported method with slight modifications[1]. In a 20 mL sealed glass vial, H_3TPO (100 mg) and $Cu(NO_3)_2 \cdot 3H_2O$ (100 mg) were added, followed by the sequential addition of DMF (4.3 mL), deionized water (4.3 mL), methanol (0.15 mL), and HNO_3 (20 μL). The resulting mixture was sonicated for 20 min and then heated at 80 °C for 48 h under solvothermal conditions, affording green transparent crystals.

Differential Scanning Calorimetry (DSC)

Adsorption enthalpies were determined using a TA Instruments DSC 25P analyzer equipped with a high-pressure gas dosing accessory. In a typical experiment, approximately 10 mg of activated **CuHTPO** was loaded into an aluminum crucible and placed in the DSC cell. Prior to gas exposure, the sample was purged with high-purity argon at 150 °C until thermal equilibrium was attained and a stable baseline was observed, followed by cooling to the testing temperature of 25 °C.

Subsequently, C_3F_6 or C_3F_8 gas was introduced under continuous flow at a partial pressure of 0.2 bar. The system was maintained under isothermal conditions until the heat flow signal returned to the baseline. The adsorption enthalpy was calculated by integrating the exothermic peak corresponding to the gas adsorption process.

Breakthrough measurements

Column breakthrough experiments were conducted in a laboratory-scale fixed-bed reactor at 25 °C. Typically, 0.70 g of activated MOF was loaded into a quartz column (4.0 mm i.d. × 300 mm) with both ends plugged by quartz wool. The packed bed was purged with helium (20 mL min^{-1}) at 150 °C for 6-12 h. After cooling to 25 °C under helium, a C_3F_6/C_3F_8 mixture (v/v = 10:90) was introduced into the column at 1 mL min^{-1}. The effluent composition was monitored continuously with an GC (HP-PONA column, FID). Regeneration was affected by flushing the column with helium (20 mL min^{-1}) at 150 °C for 2 h.

The breakthrough gas amount (q_i) was then calculated by integrating the flow rate f(t) as following equation:

$$q_i = \frac{F \times y_i \times \int_0^{t_0} f(t)dt}{m} \quad (1)$$

Where F (mL min^{-1}) is the flow rate of the gas mixture, y_i is the molar fraction of C_3F_8,

t_0 (min) is the initial breakthrough time, and m (g) is the mass of the sample Where the m represents the mass used for test.

And then the purity (c) of breakthrough gas was calculated by the following equation:

$$c(C_3F_8) = \frac{q(C_3F_8)}{0.9 * q(C_3F_8) + 0.1 * q(C_3F_6)} \quad (2)$$

in situ Infrared (IR) spectroscopy

In situ IR measurements were performed on PerkinElmer™ Frontier FT-IR spectrometer using a liquid N_2-cooled mercury cadmium telluride (MCT) detector. The spectrometer is equipped with a vacuum cell that is placed in the main compartment with the sample at the focal point of the infrared beam. To avoid the direct pressing of the MOF sample that may cause damage to the crystalline structure, the sample (~5 mg) was made into slurry form by mixing with a small amount of methanol

and pasted onto the KBr pellet. The powder sample was dried and directly attached unto KBr pellet after blowing nitrogen stream for a minute, and then transferred into the cell that is connected to different gases feeding lines and vacuum line for evacuation. The sample was activated by evacuation under vacuum at 150 ºC for 1 h, and then cooled back to room temperature for C_3F_6 and C_3F_8 adsorption measurement.

***Ab initio* calculations and simulation**

All simulations/calculations were performed using the Materials Studio 2020 package. The guest adsorption was generated from grand canonical Monte Carlo (GCMC) simulations with the fixed loading task at 298 K in the Sorption module. For GCMC simulation, the Metropolis method and universal force field (UFF) were used. All the charges of atoms were adopted Mulliken charges, which were calculated from periodic density functional theory (PDFT), and the cutoff radius was chosen as 18.5 Å for the LJ potential. The electrostatic interactions and van der Waals interactions were handled using the Ewald and Atom based summation methods, respectively, and all the equilibration steps and production steps were set as 1×10^7.

PDFT calculations were performed by the Dmol^3 module, all geometry optimizations were using the generalized gradient approximation (GGA) with the Perdew-Burke-Ernzerhof (PBE) functional and the double numerical plus d-functions (DNP) basis set, grimme for DFT-D correction, and the Effective Core Potentials (ECP). The energy, gradient and displacement convergence criteria were set as 1×10^{-5} Ha, 2×10^{-3} Å and 5×10^{-3} Å, respectively. The host-guest binding energy ($\Delta E_{binding}$) was calculated by:

$$\Delta E_{binding} = E_{host+guest} - E_{hos} - E_{guest}$$

where the $E_{host+guest}$ is the energy of the final host-guest system, the E_{host} and E_{guest} are the energies of the host and guest, respectively.

The energy barriers were obtained by calculating transition state energies through the climbing-image nudged elastic band (CI-NEB) method. The optimized host-guest structures from GCMC were defined as state I, and its system energy was set as the reference. The transition state, defined as state II, search calculations were conducted to identify transition states associated with guest transport between the two energy minimum configurations. State III represented the final state where guests were diffused into the next preferential site of optimized host-guest structures. The energy barrier was calculated by $E_a = E_{II} - E_I$.

Isotherm fitting and calculation of adsorption heat

$$q = \frac{a_1 * b_1 * P^{c_1}}{1 + b_1 * P^{c_1}} + \frac{a_2 * b_2 * P^{c_2}}{1 + b_2 * P^{c_2}} \quad (1)$$

$$Q_{st} = -R\left(\frac{\partial lnP}{\partial(1/T)}\right)_p \quad (2)$$

The above virial expression was used to fit the combined isotherm data for **CuHTPO** at 273, 283, 298 and 303 K (P is the pressure, q is the adsorbed amount a_i Maximum adsorption capacity of site i, T is the temperature, b_i is Affinity constant and c_i is Heterogeneity parameter). Q_{st} is the coverage-dependent enthalpy of adsorption and R is the universal gas constant.

IAST Selectivity

The experimental isotherm data for pure gas A, and gas B were fitted at 298 K using a dual-site Langmuir-Freundlich (DSLF) model:

$$q = \frac{a_1 * b_1 * P^{c_1}}{1 + b_1 * P^{c_1}} + \frac{a_2 * b_2 * P^{c_2}}{1 + b_2 * P^{c_2}} \quad (1)$$

Where q and p were adsorbed amounts and the pressure of component *i*, respectively.

The adsorption selectivities for binary mixtures of gas A/gas B, defined by

$$S_{i/j} = \frac{x_i * y_j}{x_j / y_i} \quad (3)$$

was calculated using the Ideal Adsorption Solution Theory (IAST) of Myers and Prausnitz, where x_i is the mole fraction of component *i* in the adsorbed phase and y_i is the mole fraction of component *i* in the bulk.

Table S1. Comparison of physicochemical properties of C_3F_6 and C_3F_8[2-4].

Compounds	Dimensions (10^{-10} m)	Boiling point (K)	Melting point (K)	Dipole moment (μ)	Polarizability ($\times10^{-24}$ cm^3)
C_3F_6	7.3 × 6.2 × 5.1	242	120.4	0.023 D	6.59
C_3F_8	7.6 × 5.3 × 5.1	236.3	90	0 D	6.80

Table S2. Summary of C_3F_6 and C_3F_8 adsorption and separation performance by representative MOFs at 298 K[4].

Porous solids	C_3F_6 uptakes at 100 kPa ($cm^3\ g^{-1}$)	C_3F_8 uptakes at 100 kPa ($cm^3\ g^{-1}$)	C_3F_6/C_3F_8 uptake ratio	Qst ($kJ\ mol^{-1}$)
$Ni(INA)_2$-NH_2[4]	56.7	5.3	10.5	52.7
Al-PMA[5]	39.3	1.1	37.3	56.8
Zr-PMA[6]	59.1	17.0	3.5	36.1
Zn-bzc-CF_3[7]	47.0	1.6	30	44.2
JXNU-21[8]	31.2	17.0	1.8	34.8
Ca-tcpb[9]	44.8	1.3	33.3	48.3
CoFA[10]	44.8	3.6	12.5	33.1
Mn-dhbp[11]	44.6	3.6	12.4	47.8
CuHTPO (This work)	**71.6**	**1.5**	**47.7**	43.0

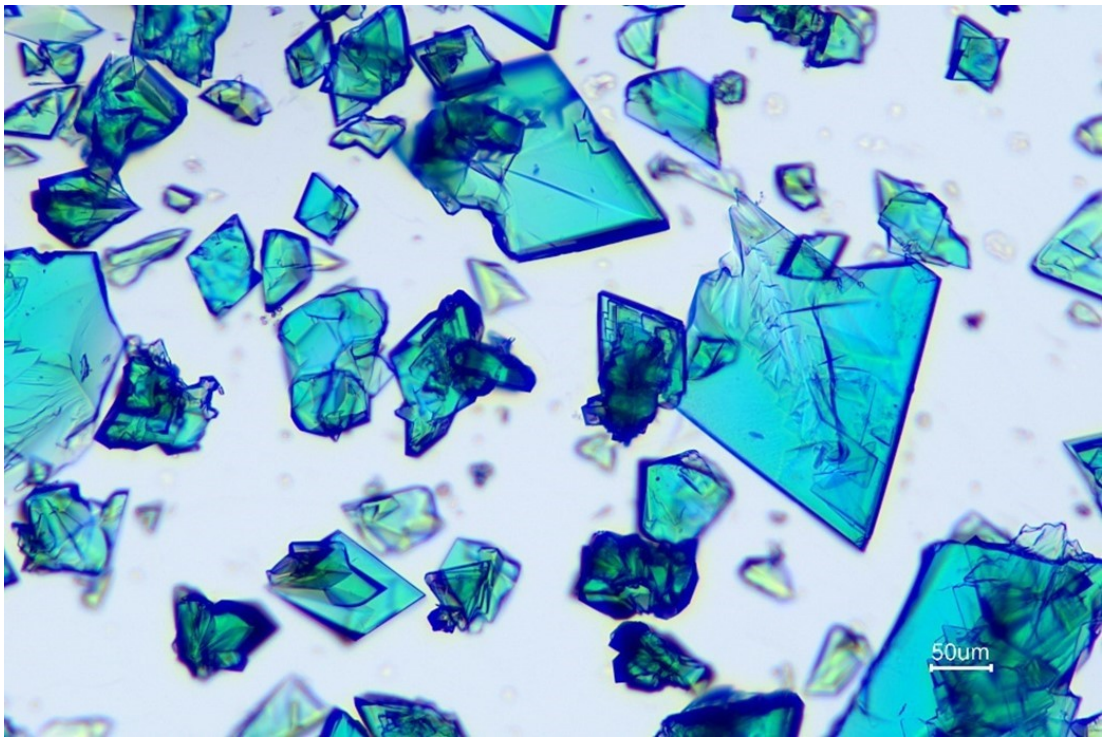

Fig. S1 Optical microscope image of the as-synthesized crystals of **CuHTPO**.

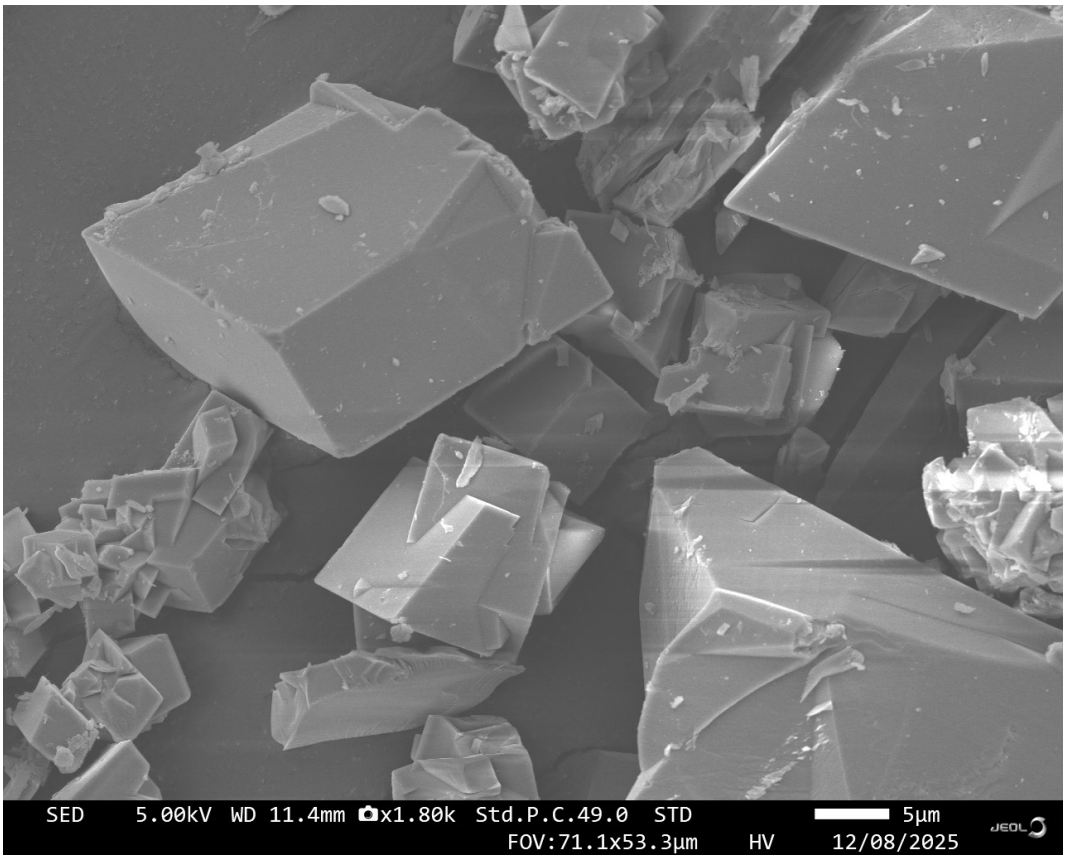

Fig. S2 SEM image for **CuHTPO**.

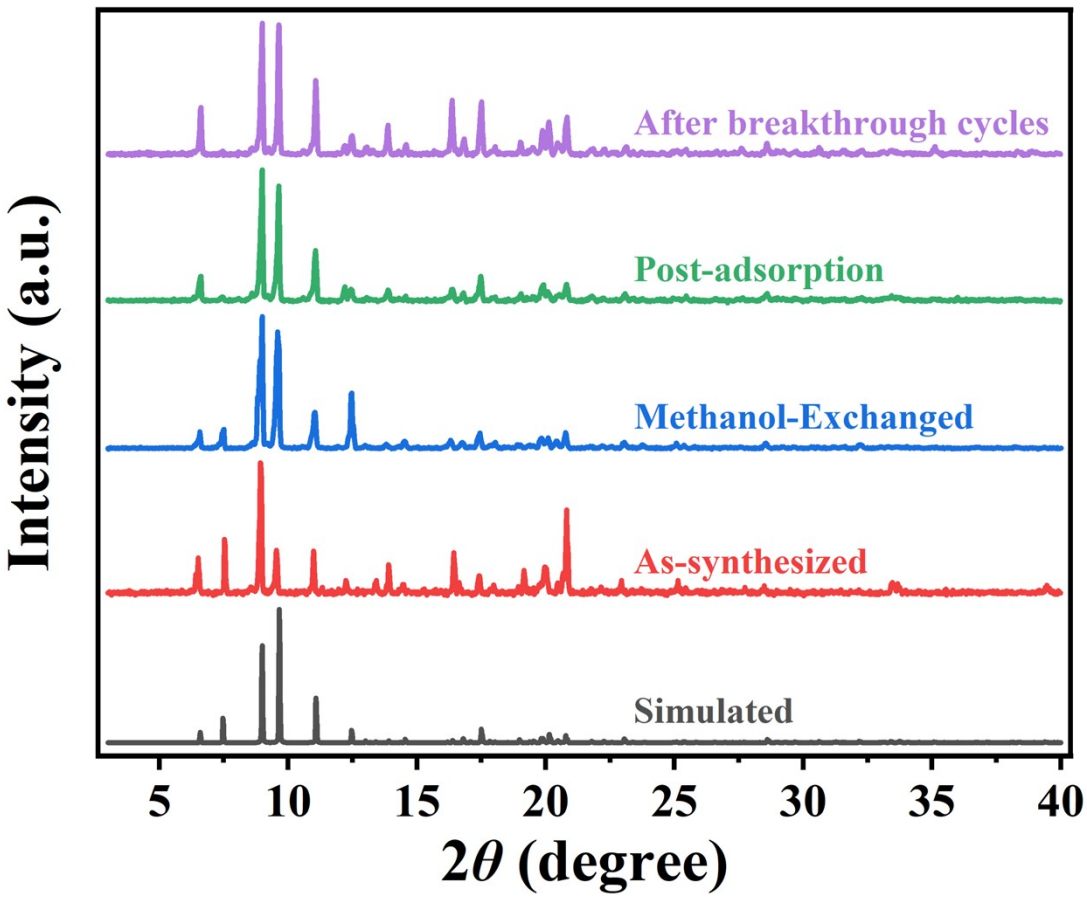

Fig. S3 Simulated and experimental PXRD patterns of **CuHTPO**.

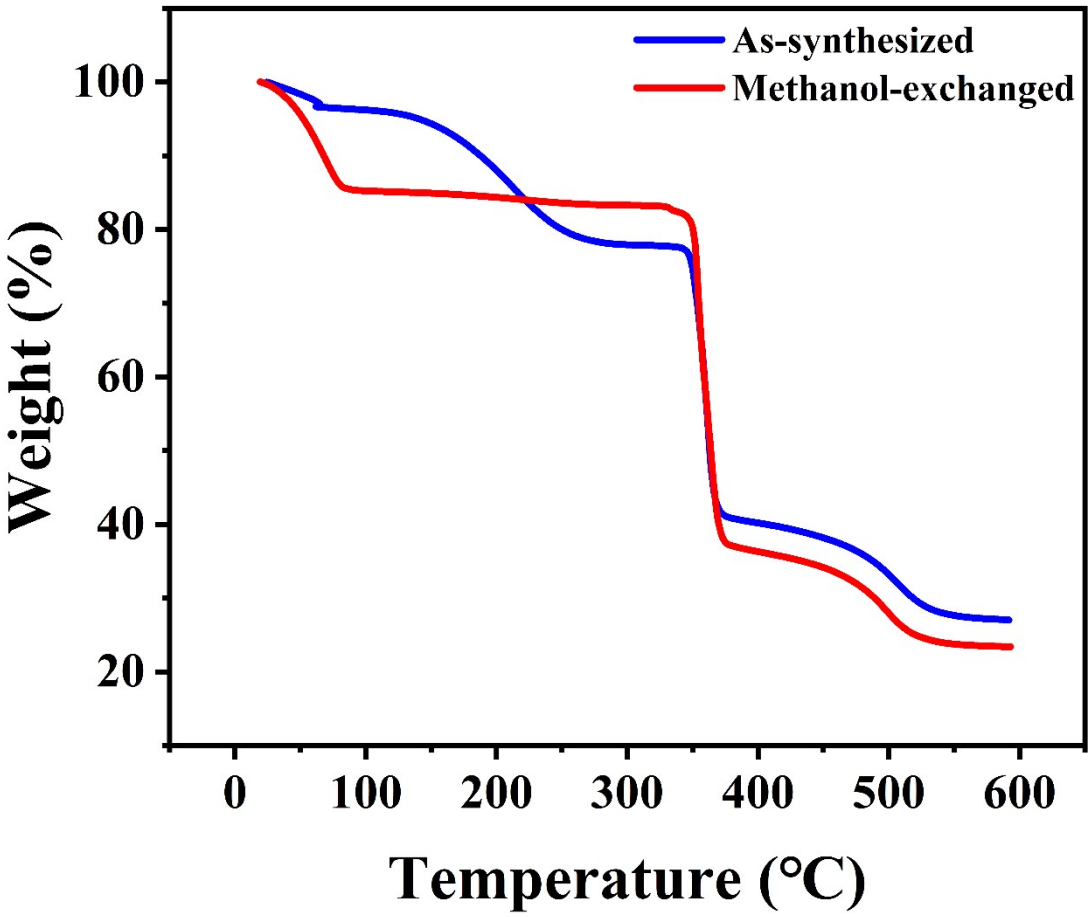

Fig. S4 TGA curves of as-synthesized and methanol-exchanged samples of **CuHTPO**.

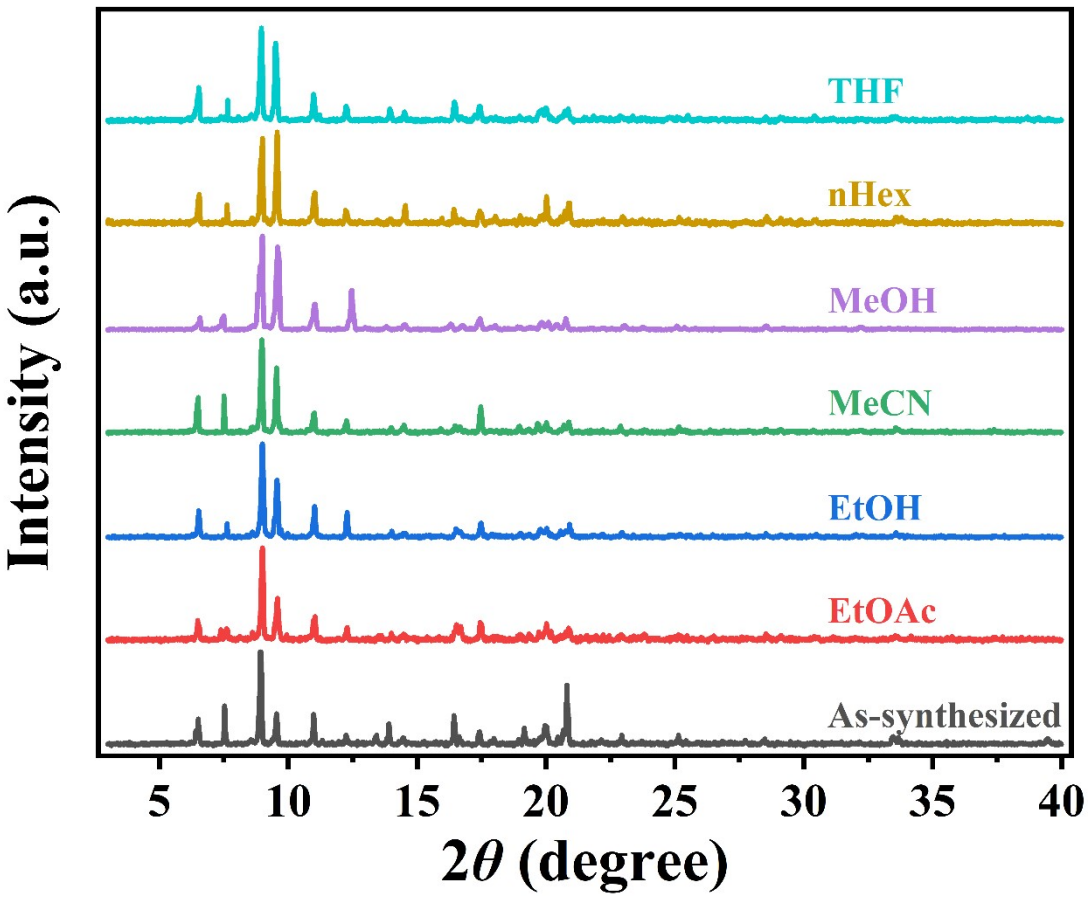

Fig. S5 PXRD patterns of **CuHTPO** recorded after immersion in various organic solvents for 7 days, compared with the simulated pattern.

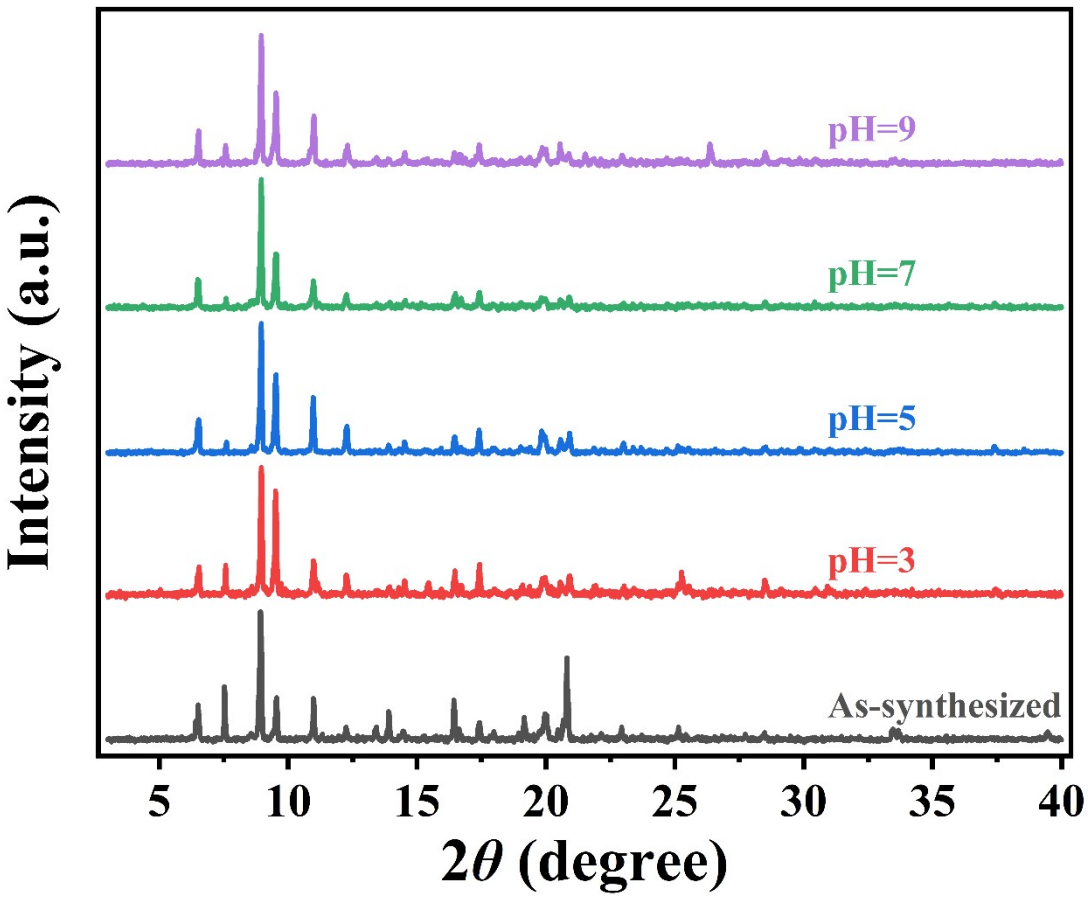

Fig. S6 PXRD patterns of **CuHTPO** recorded after immersion in aqueous solutions with varying pH values (pH = 3 to 9) for seven days, compared with the simulated pattern.

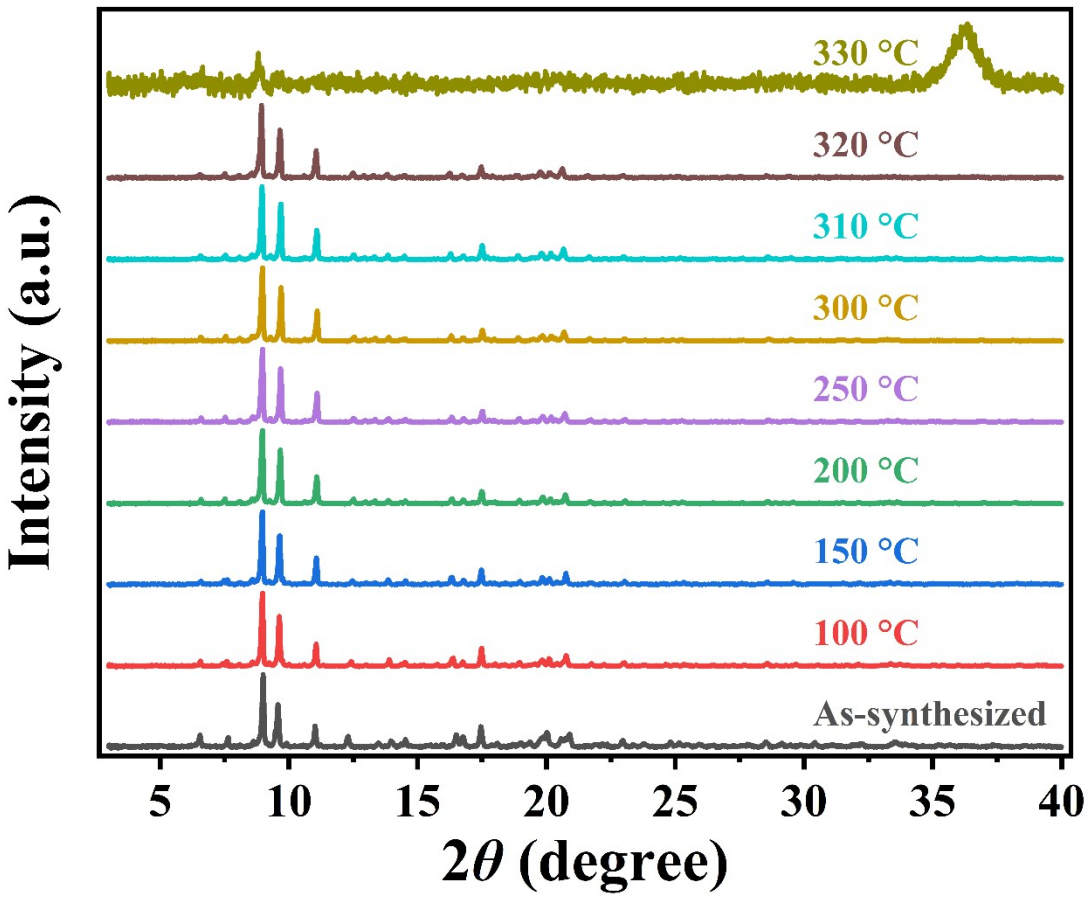

Fig. S7 Variable-temperature in situ PXRD patterns of **CuHTPO** under a nitrogen atmosphere.

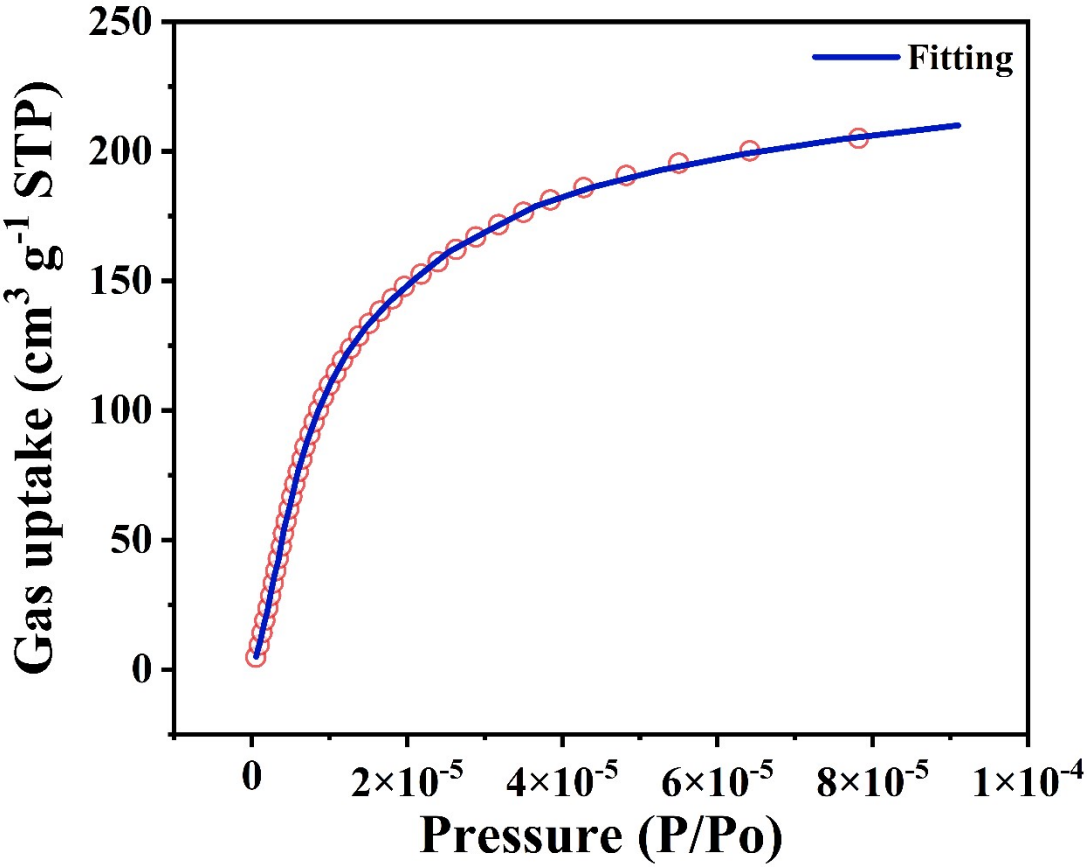

Fig. S8 N_2 adsorption isotherm at 77 K fitted using the NLDFT method.

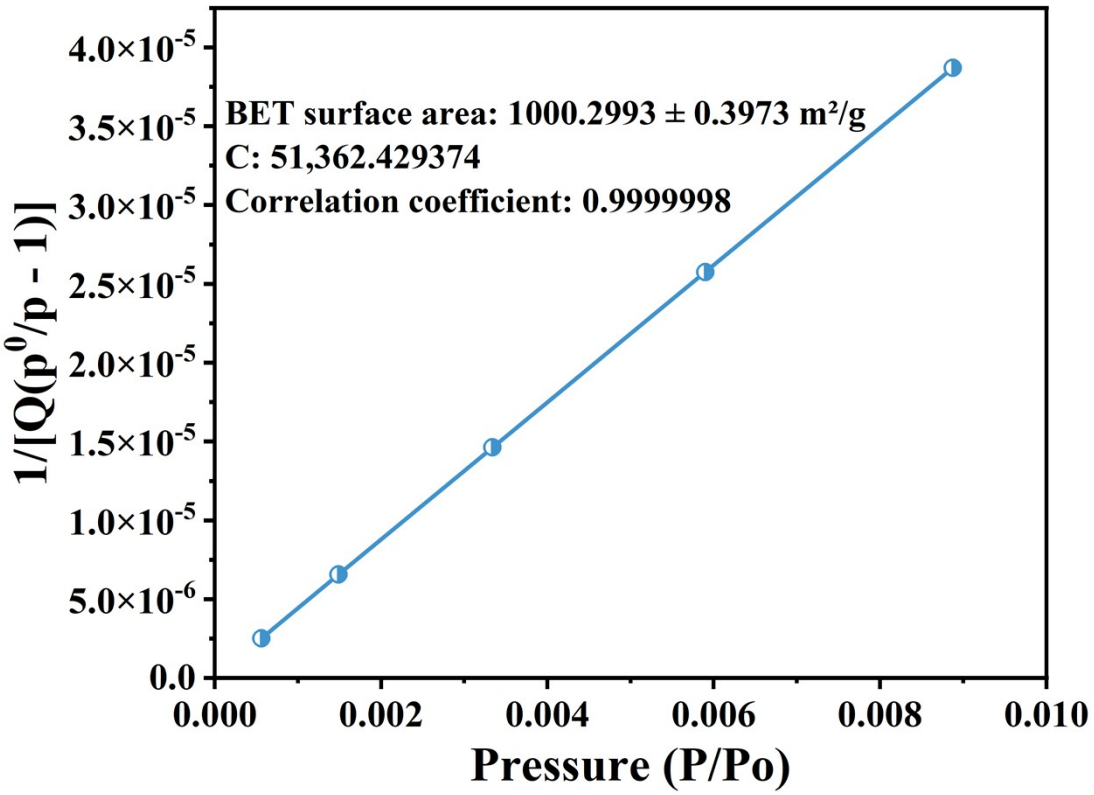

Fig. S9 Fitting of BET surface area of **CuHTPO** calculated from N_2 adsorption isotherms measured at 77 K.

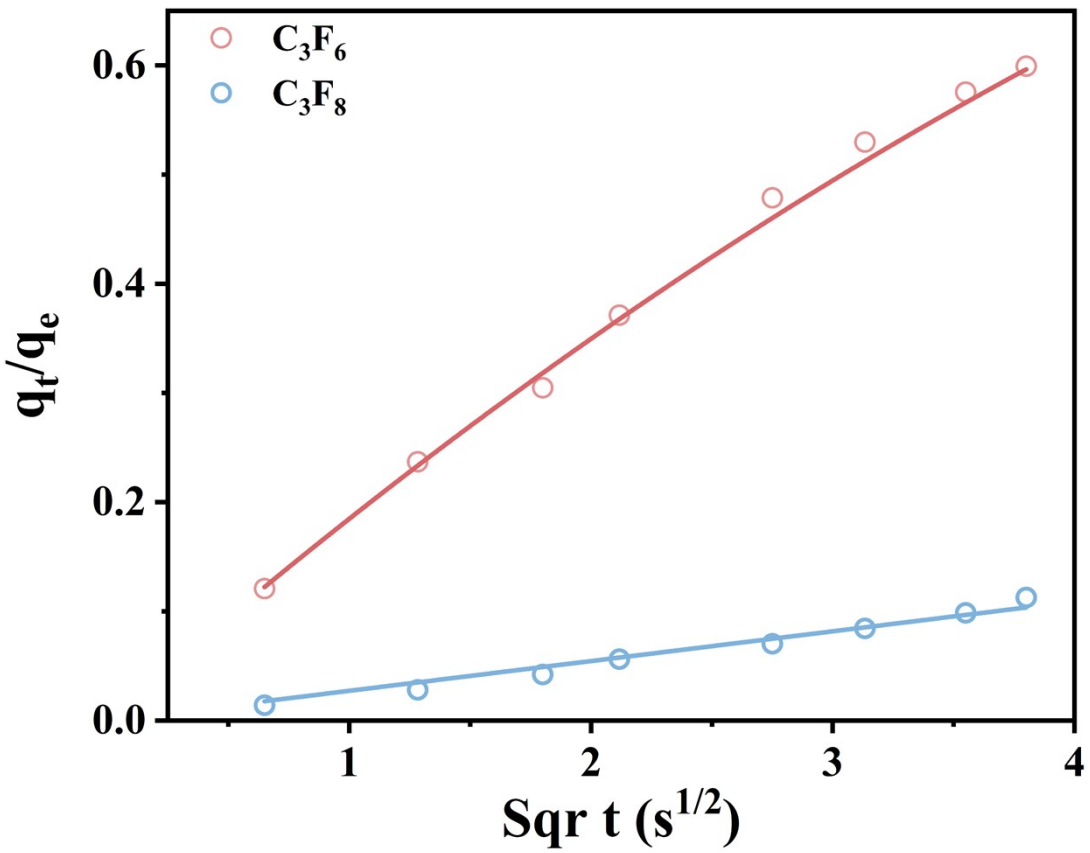

Fig. S10 Time-dependent adsorption profiles of C_3F_6 and C_3F_8 on **CuHTPO** at 298 K.

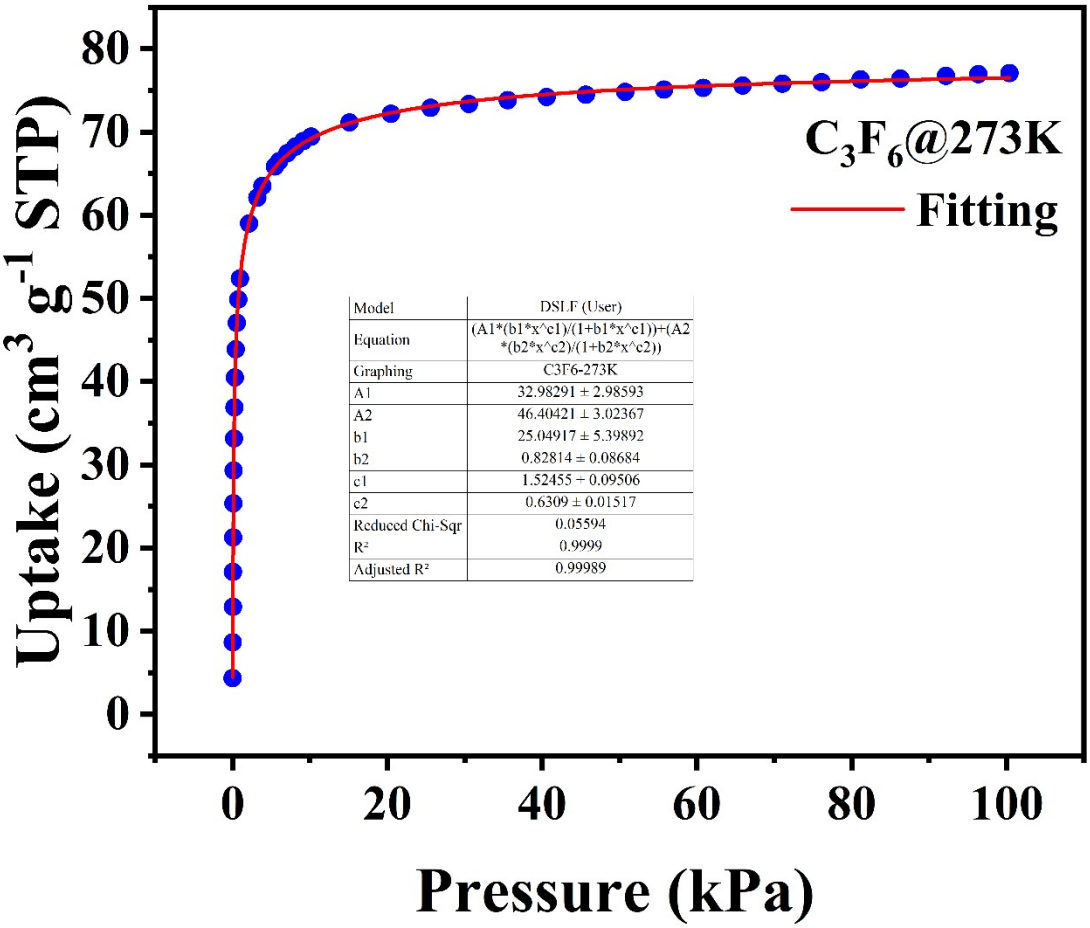

Model	DSLF (User)
Equation	(A1*(b1*x^c1)/(1+b1*x^c1))+(A2*(b2*x^c2)/(1+b2*x^c2))
Graphing	C3F6-273K
A1	32.98291 ± 2.98593
A2	46.40421 ± 3.02367
b1	25.04917 ± 5.39892
b2	0.82814 ± 0.08684
c1	1.52455 ± 0.09506
c2	0.6309 ± 0.01517
Reduced Chi-Sqr	0.05594
R^2	0.9999
Adjusted R^2	0.99989

Fig. S11 Fitting curves of C_3F_6 at 273 K using the dual-site Langmuir-Freundlich (DSLF) equation and the corresponding fitting parameters.

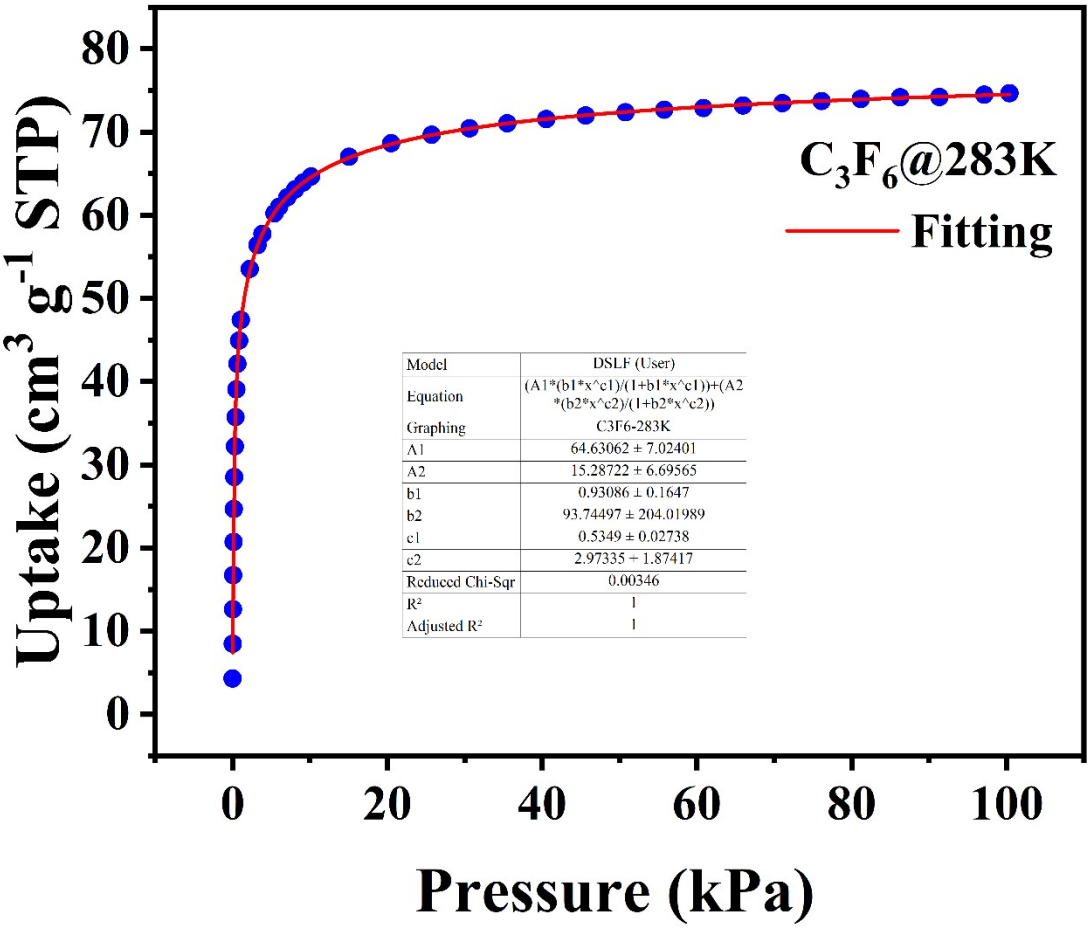

Fig. S12 Fitting curves of C_3F_6 at 283 K using the dual-site Langmuir-Freundlich (DSLF) equation and the corresponding fitting parameters.

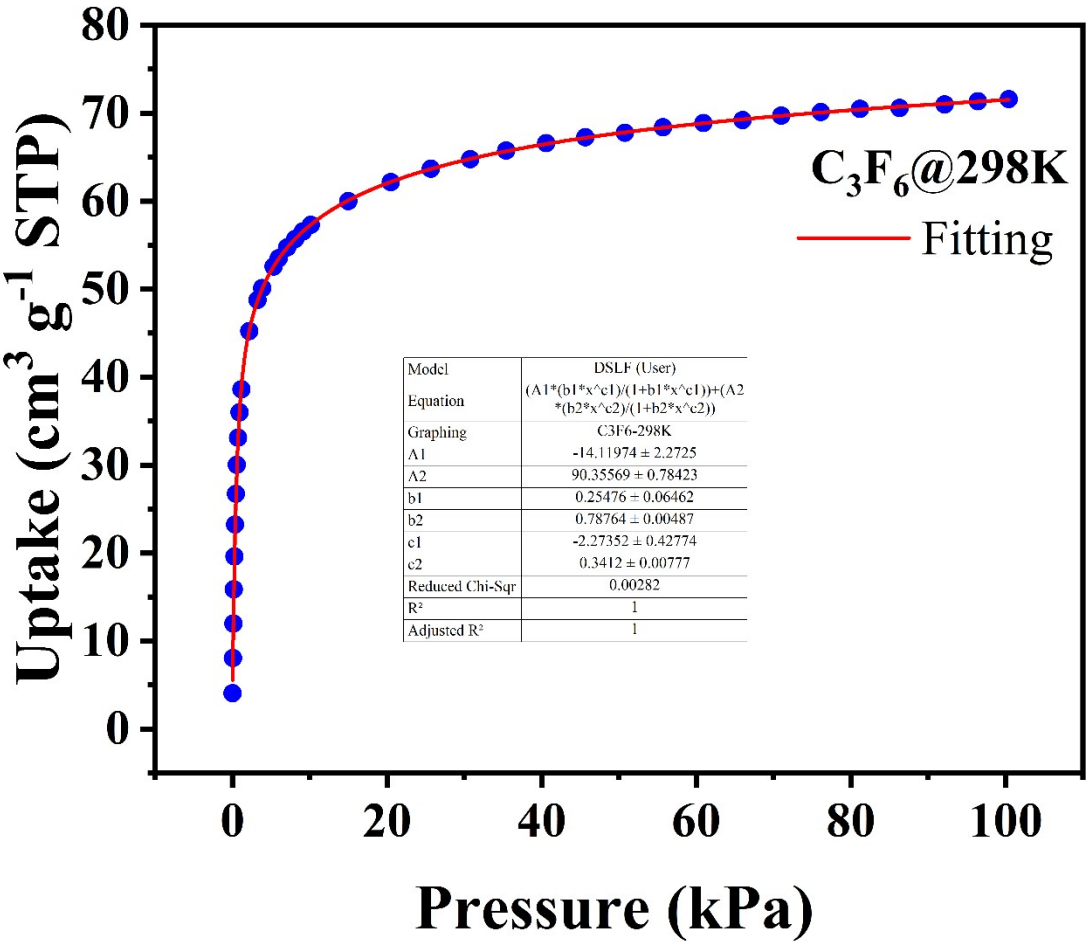

Fig. S13 Fitting curves of C_3F_6 at 298 K using the dual-site Langmuir-Freundlich (DSLF) equation and the corresponding fitting parameters.

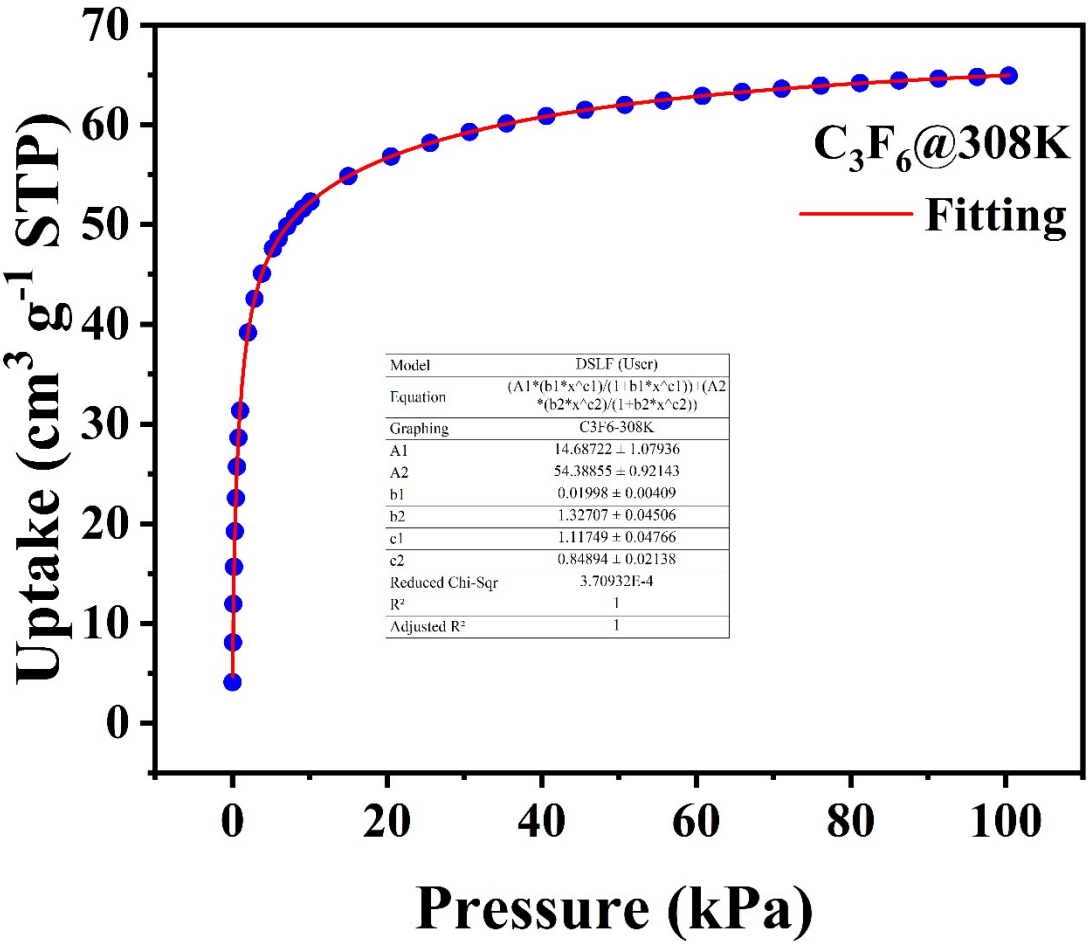

Fig. S14 Fitting curves of C_3F_6 at 308 K using the dual-site Langmuir-Freundlich (DSLF) equation and the corresponding fitting parameters.

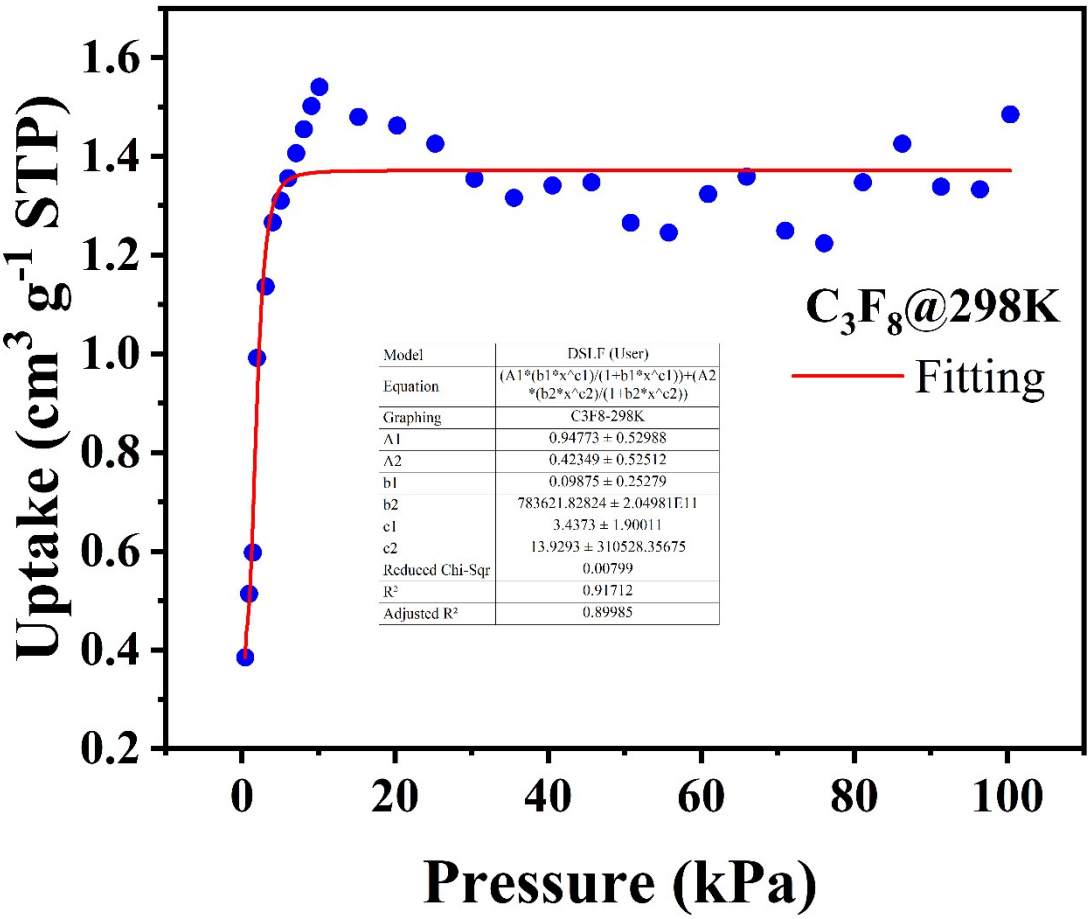

Fig. S15 Fitting curves of C_3F_8 at 298 K using the dual-site Langmuir-Freundlich (DSLF) equation and the corresponding fitting parameters.

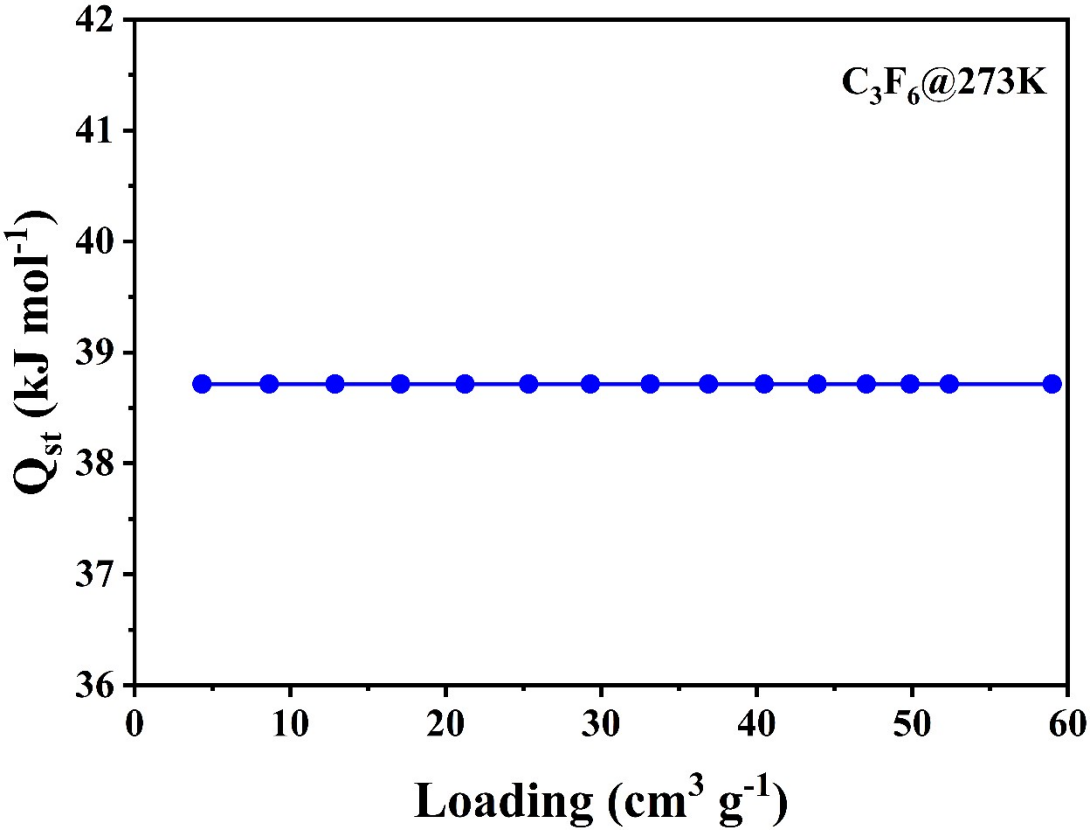

Fig. S16 Isosteric heat of adsorption (Q_{st}) derived from adsorption isotherms.

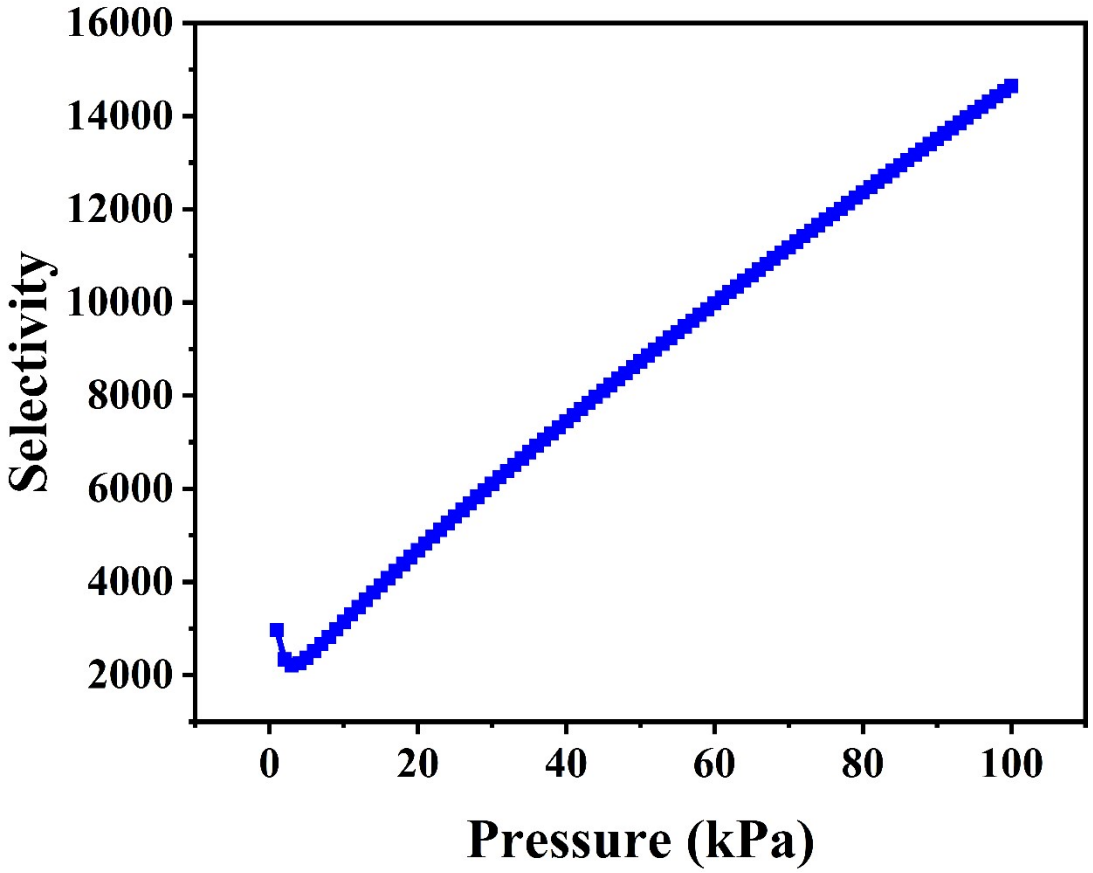

Fig. S17 IAST selectivity of C_3F_6/C_3F_8 (10:90, v/v) calculated from the 298 K isotherms.

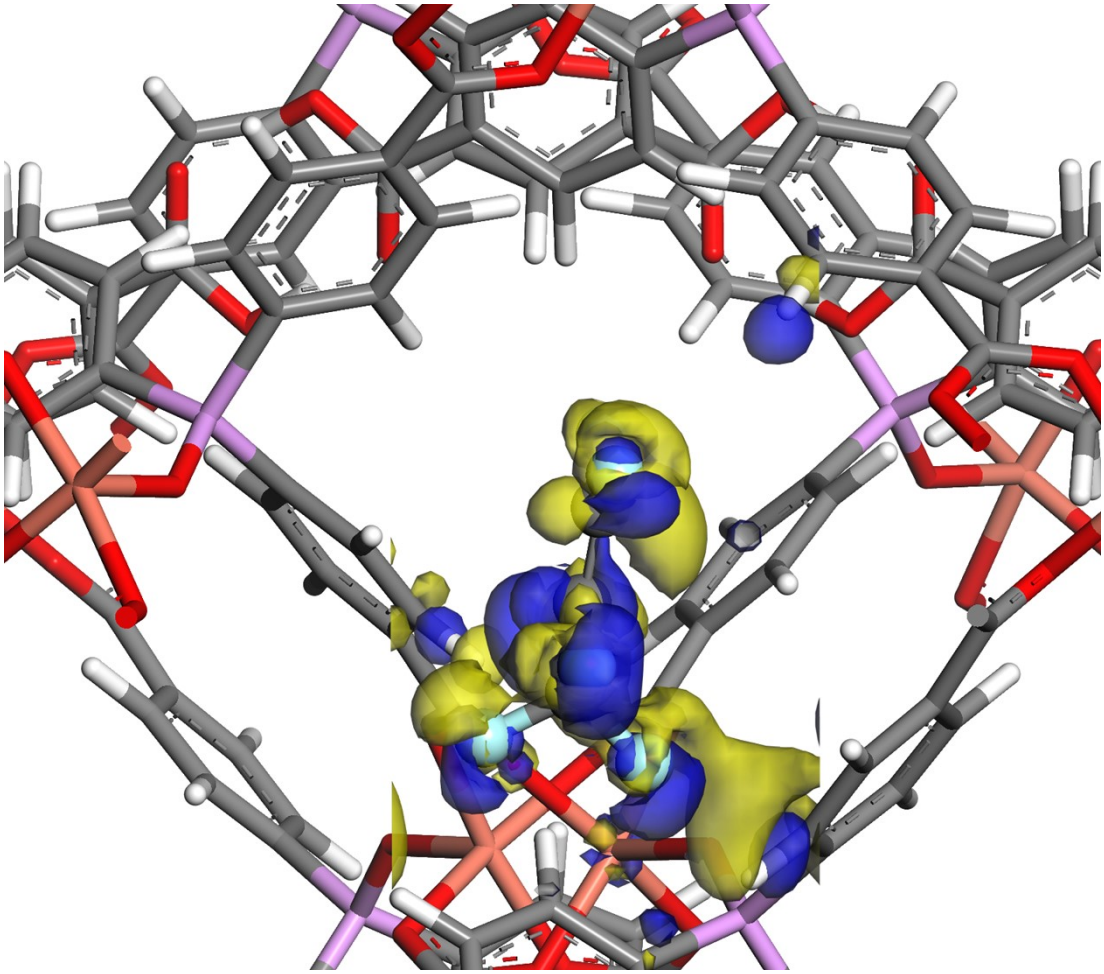

Fig. S18 Charge density difference plot of C_3F_6-adsorbed **CuHTPO**.

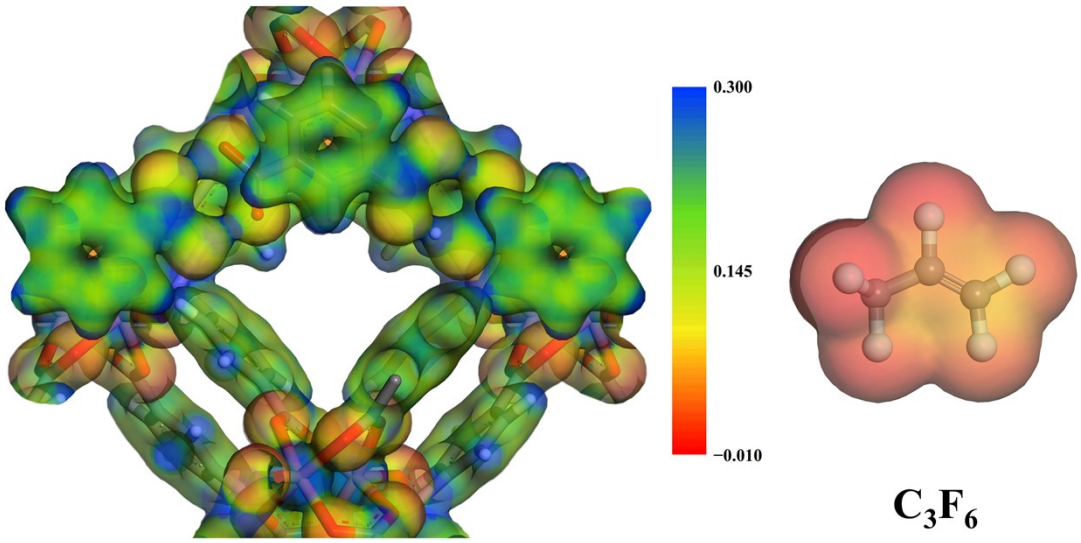

Fig. S19 Electrostatic potential (ESP) surfaces of **CuHTPO** and C_3F_6. Red and blue regions represent electron-rich and electron-deficient areas, respectively.

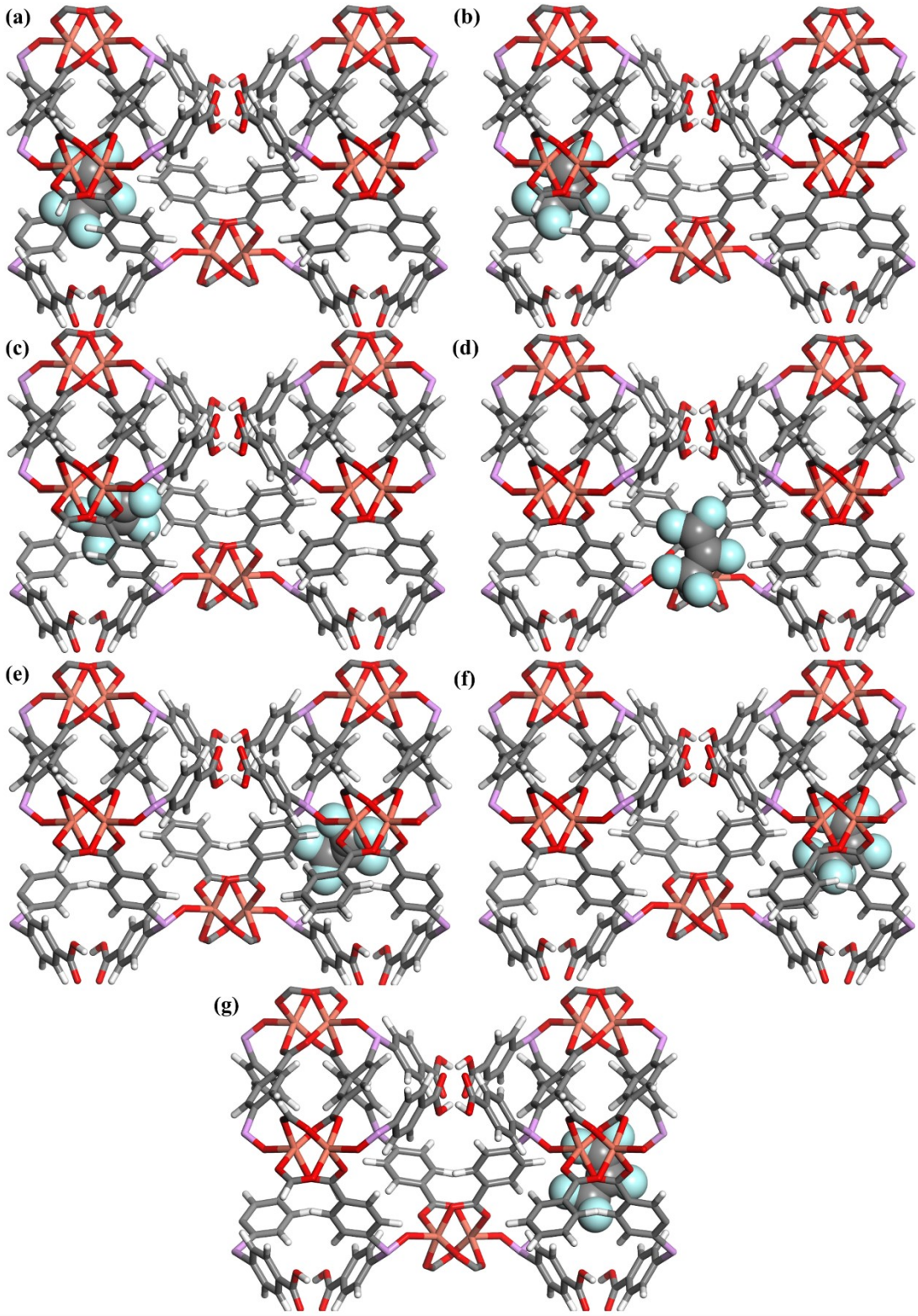

Fig. S20 (a)-(g) DFT-optimized structural models and corresponding energy barriers for C_3F_6 diffusion into the **CuHTPO** pore along the diffusion pathway, with diffusion coordinates ranging from 0% to 100%.

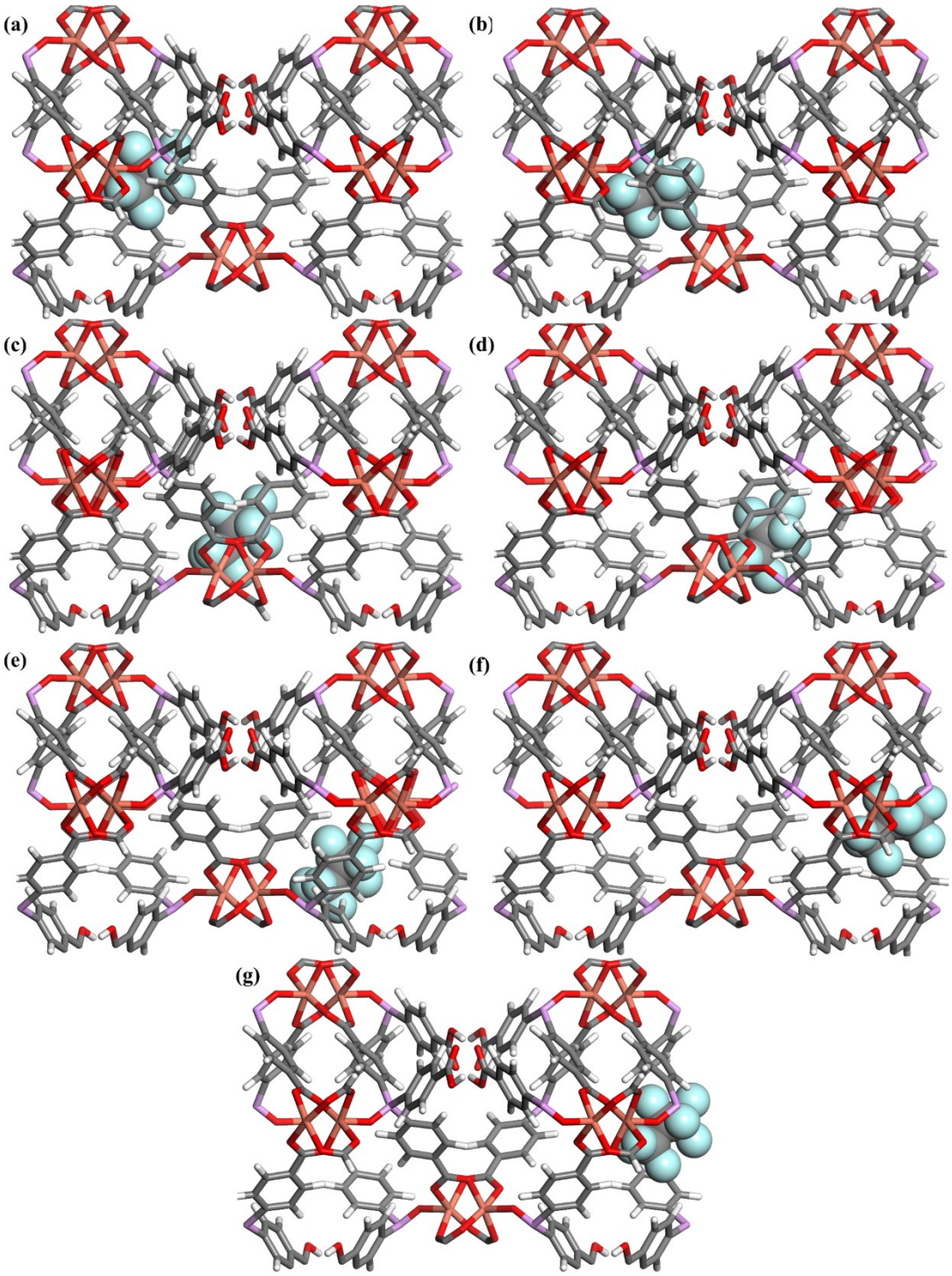

Fig. S21 (a)-(g) DFT-optimized structural models and corresponding energy barriers for C_3F_8 diffusion into the **CuHTPO** pore along the diffusion pathway, with diffusion coordinates ranging from 0% to 100%.

References

1 W. R. Lee, D. W. Ryu, W. J. Phang, J. H. Park and C. S. Hong, *Chem. Commun.*, 2012, **48**, 10847.

2 D. O'Hagan, *Chem. Soc. Rev.*, 2008, **37**, 308-319.

3 C. J. Schack and K. O. Christe, *Inorg. Chem.*, 1979, **18**, 2619-2620.

4 X. Lv, M. Zheng, Z. Jiang, H. Huang, Z. Bao and C. Zhong, *Chem. Eng. J.*, 2025, **522**, 168005.

5 W. Xia, Z. Zhou, L. Sheng, L. Chen, F. Zheng, Z. Zhang, Q. Yang, Q. Ren and Z. Bao, *Science Bulletin*, 2025, **70**, 232-240.

6 W. Xia, Z. Zhou, C. Xia, L. Chen, L. Sheng, F. Zheng, Z. Zhang, Q. Yang, Q. Ren and Z. Bao, *Angew. Chem. Int. Ed.*, 2025, **64**, e202503505.

7 M. Zheng, W. Xue, T. Yan, Z. Jiang, Z. Fang, H. Huang and C. Zhong, *Angew. Chem. Int. Ed.*, 2024, **63**, e202401770.

8 Y.-Q. Feng, H.-F. Ma, S. Luo, H.-P. Xiao, Q.-Y. Liu and Y.-L. Wang, *Inorg. Chem. Front.*, 2025, **12**, 623-629.

9 W. Xia, Y. Yang, L. Sheng, Z. Zhou, L. Chen, Z. Zhang, Z. Zhang, Q. Yang, Q. Ren and Z. Bao, *Sci. Adv.*, 2024, **10**, eadj6473.

10 W. Xia, Z. Zhou, L. Sheng, L. Chen, F. Shen, F. Zheng, Z. Zhang, Q. Yang, Q. Ren and Z. Bao, *Nat. Commun.*, 2024, **15**, 8716.

11 L. Sheng, W. Xia, Y. Fu, J. Yan, Z. Zhou, F. Zheng, F. Shen, L. Chen, Z. Zhang, Q. Yang, Q. Ren and Z. Bao, *ACS Mater. Lett.*, 2025, **7**, 2080-2087.